



**HAL**  
open science

# Phenomenological study of parabolic and spherical indentation of elastic-ideally plastic material

Olivier Bartier, Xavier Hernot

► **To cite this version:**

Olivier Bartier, Xavier Hernot. Phenomenological study of parabolic and spherical indentation of elastic-ideally plastic material. *International Journal of Solids and Structures*, 2012, 49, pp.2015-2026. 10.1016/j.ijsolstr.2012.04.005 . hal-00861520

**HAL Id: hal-00861520**

**<https://univ-rennes.hal.science/hal-00861520>**

Submitted on 12 Sep 2013

**HAL** is a multi-disciplinary open access archive for the deposit and dissemination of scientific research documents, whether they are published or not. The documents may come from teaching and research institutions in France or abroad, or from public or private research centers.

L'archive ouverte pluridisciplinaire **HAL**, est destinée au dépôt et à la diffusion de documents scientifiques de niveau recherche, publiés ou non, émanant des établissements d'enseignement et de recherche français ou étrangers, des laboratoires publics ou privés.

# Phenomenological study of parabolic and spherical indentation of elastic-ideally plastic material

O. Bartier<sup>a</sup>, X. Hernot<sup>b</sup>

<sup>a</sup> L.A.R.M.A.U.R, E.A. 42.82, Bât 10B, Université de Rennes 1, Campus de Beaulieu, 35402 Rennes Cedex, France. Olivier.bartier@univ-rennes1.fr

<sup>b</sup> L.A.R.M.A.U.R, E.A. 42.82, Bât 10B, Université de Rennes 1, Campus de Beaulieu, 35402 Rennes Cedex, France. Xavier.hernot@univ-rennes1.fr

Corresponding author : Olivier.bartier, Tel: +33 2 2323 6148; fax: +33 2 2323 6111 *E-mail address*: Olivier.bartier@univ-rennes1.fr L.A.R.M.A.U.R, E.A. 410, Bât 10B, Université de Rennes 1, Campus de Beaulieu, 35402 Rennes Cedex, France.

## abstract

A phenomenological study of parabolic and spherical indentation of elastic ideally plastic materials was carried out by using precise results of finite elements calculations. The study shows that no “pseudo-Hertzian” regime occurs during spherical indentation. As soon as the yield stress of the indented material is exceeded, a deviation from the, purely elastic Hertzian contact behaviour is found. Two elastic-plastic regimes and two plastic regimes are observed for materials of very large Young modulus to Yield stress ratio,  $E/\sigma_y$ . The first elastic-plastic regime corresponds to a strong evolution of the indented plastic zone. The first plastic regime corresponds to the commonly called “fully plastic regime”, in which the average indentation pressure is constant and equal to about three times the yield stress of the indented material. In this regime, the contact depth to penetration depth ratio tends toward a constant value, i.e.  $h_c/h=1.47$ .  $h_c/h$  is only constant for very low values of yield strain ( $\sigma_y/E$  lower than  $5 \cdot 10^{-6}$ ) when  $aE^*/R\sigma_y$  is higher than 10,000. The second plastic regime corresponds to a decrease in the average indentation pressure and to a steeper increase in the pile-up. For materials with very large  $E/\sigma_y$  ratio, the second plastic regime appears when the value of the non-dimensional contact radius  $a/R$  is lower than 0.01. In the case of spherical and parabolic indentation, results show that the first plastic regime exists only for elastic-ideally plastic materials having an  $E/\sigma_y$  ratio higher than approximately 2.000.

Keywords: Spherical indentation; deformation regime; elastic ideally plastic material; finite element method

## 1. Introduction

A characteristic feature of the spherical indentation is that different regimes can occur during the deformation of metals. So far, elastic, elastic-plastic with elastically-dominated and plastically dominated parts, fully plastic and finite deformation regimes were observed for spherical indentation (Hertz, 1881; Tabor, 1951; Johnson, 1985; Mesarovic and Fleck, 1999; Park and Pharr, 2004, Pane and Blank, 2006). The deformation process produced during spherical indentation is well described if the regime is elastic, but this is more complex when plasticity occurs. Many experimental and numerical studies have been performed in order to understand the phenomena which occur during spherical indentation. Following the early work of Tabor (1951), Johnson (1985) suggested that the spherical indentation process can be divided into three distinct regimes: elastic, elastic-plastic and fully plastic. When the yield point is first exceeded the plastic zone is small and fully contained by material which remains

elastic so that the plastic strains are of the same order of magnitude as the surrounding elastic strains. In these circumstances the material displaced by the indenter is accommodated by an elastic expansion of the surrounding solid. As the indentation becomes more severe, either by increasing the load, an increasing pressure is required beneath the indenter to produce the necessary expansion. Eventually the plastic zone reaches the free surface and the material is free to move by plastic flow to the sides of the indenter. This is the “uncontained” mode of deformation analysed by the theory of rigid-plastic solids proposed by Ishlinsky (1944) which used the slip-line method, as well as Hill et al (1989) and Biwa and Storåkers (1995) which used deformation and flow theory, respectively. It is assumed that the two ranges of loading, ie elastic-plastic and fully plastic, correspond respectively to the “contained” and “uncontained” modes. For the “uncontained” mode, the elasticity is considered as negligible. According to the similarity solution proposed for the “uncontained mode” (Biwa and Storåkers, 1995), the upper limit of the mean contact pressure, which is usually interpreted as the material hardness, is equal to three times the yield strength of an elastic ideally plastic material. In the elastic-plastic regime, the mean contact pressure starts from a value equal to  $1.07\sigma_y$  and reaches the value of the similarity solution. The ratio between the mean contact pressure,  $P_m$ , and the yield stress corresponds to the “constraint factor” called  $\psi$ , which is commonly used to study the transition between elastic-plastic and “fully” plastic regime. On the basis of results of different experimental and numerical indentation tests using spheres, Johnson (1985) showed that fully plastic deformation is reached at a value  $\Lambda = E^*a/(\sigma_y R) \approx 40$ . For elastic-ideally plastic solids,  $\psi$  increases until the ratio  $E^*a/(\sigma_y R)$  is equal to 40–50 (Mesarovic and Fleck, 1999). More recently, for a range of  $E^*/\sigma_y$  ratio, which includes most metals, Park and Pharr (2004) showed that full plasticity is achieved when the value of the ratio  $E^*a/(\sigma_y R)$  is equal to 50-200. For elastic– ideally plastic materials of  $E/\sigma_y$  ratio in the range 20-1500, which covers most metals, ceramics, and glasses, the results suggest that fully developed plasticity, as conventionally defined by the point at which the constraint factor levels off at a value of about 3, starts at the much higher value  $E^*a/(\sigma_y R) = 110$  (Taljat and Pharr, 2004). Lastly, in a study of the role of plasticity in spherical indentation for different kinematic and isotropic materials, the limit between the elastic-plastic regime and the fully plastic regime was fixed at  $E^*a/(\sigma_y R) = 80$  by Pane and Blank (2006).

Another parameter,  $c^2$ , and equal to  $a^2/(2hR)$ , is also used in order to study the deformation regimes. This parameter was proposed in order to quantify the degree of piling-up and sinking-in during the indentation test.  $c^2 > 1$  indicates piling-up, whereas  $c^2 < 1$  accounts for sinking-in (Matthews, 1980; Hill et al, 1989; Taljat et al., 1998; Alcalá et al., 2000; Kucharski and Mröz, 2001). In the case of material elastically deformed by indentation,  $c^2$  is constant and equal to 0.5. When the stress under the indenter is higher than the yield stress of the indented material, this parameter increases with the indent depth during a stage called “elastic-plastic indentation regime” (Mesarovic and Fleck, 1999). For higher indent depths, the  $c^2$  parameter is again considered constant during the stage called “fully plastic regime” ((Matthews, 1980; Hill et al, 1989; Taljat et al., 1998; Alcalá et al., 2000). For indentation by a sphere, Bower et al (1993) and Mesarovic and Fleck (1999) show that the fully plastic regime can be subdivided into two regimes. For relatively small contact sizes, a similarity solution applies while for large contact sizes, a finite deformation mode dominates. Mesarovic and Fleck (1999) define the first regime: “plastic similarity regime”, in which  $\psi$  and  $c^2$  are constant. By observing the results of Mesarovic and Fleck (1999), we can notice a difference between the lower limit of the “fully plastic regime“ determined by  $c^2$  and the lower limit of the “plastic similarity regime” determined by  $\psi$  and  $c^2$ . For example, in the case of  $E^*/\sigma_y$  ratio equal to 10000,  $\psi$  is constant when  $E^*a/(\sigma_y R)$  is equal to about 40-50 and  $c^2$  is constant when  $E^*a/(\sigma_y R)$  reaches the value of 1000. The second regime inside the “fully plastic regime”,

called “finite deformation regime” by Mesarovic and Fleck (1999), occurs for large contact sizes and corresponds to a drop of  $\psi$  and  $c^2$ . For smaller  $E^*/\sigma_y$  ratios, Mesarovic and Fleck (1999) showed that the plastic similarity regime is never reached since  $c^2$  increases in the elastic-plastic regime and immediately falls with increasing contact size in the stage called “finite deformation regime”. For Bower et al. (1993) and Mesarovic and Fleck (1999), the drop in  $c^2$  value for large contact sizes represents the failure of the assumptions involved in the similarity solution, especially the assumption of infinitesimal strain kinematics (Bower et al., 1993; Mesarovic and Fleck, 1999) and the boundary condition of uniform normal velocity (Mesarovic and Fleck, 1999). We can notice that the similarity solution was also determined with the assumption that the geometric profile of the indenter can be represented by a power-law relationship. This assumption includes indentation by a rigid sphere, since, for small contact sizes, the profile of a sphere can be approximated by a paraboloid of revolution. For large contact sizes, the failure of this assumption in the case of spherical indentation can also explain the drop in the  $a^2/2hR$  ratio. Indeed, in a recent study, Hernot et al. (2006) showed that the use of the  $c^2$  parameter has for consequence a noticeable underestimation of the contact radius for large values of penetration depth because the spherical indenter cannot be considered as similar to the parabolic indenter.

The aim of this work is to study the different indentation regimes during parabolic and spherical indentation of elastic-ideally plastic materials on the basis of precise numerical simulations. For our study, we propose to analyse the evolution of the constraint factor  $\psi$ , the contact depth-penetration depth ratio ( $h_c/h$ ), the  $c^2$  parameter and two non-dimensional expressions  $(dF/da).(a/F)$  and  $(da/dh).(h/a)$  during the indentation test. The expansion of the plastic deformation in the indented zone and the location of the maximum plastic deformation will be also studied in this work. In a first step, the analysis is carried out by using the results of numerical simulations of the indentation of an elastic-plastic half-space by a frictionless rigid paraboloid of revolution. This type of indenter is used for the same reason as mentioned before in a previous study (Hernot et al. (2006)). In a second step, some numerical simulations are performed in the case of a rigid spherical indenter in order to study the influence of the shape of the indenter on the indentation regimes for high contact radius values. Another goal of the proposed paper is to validate the use of the non dimensional expressions  $(dF/da).(a/F)$  and  $(da/dh).(h/a)$  for the study the indentation of elastic-ideally plastic materials. This work is the first step before studying the indentation regimes during spherical indentation of work hardened materials by using the non-dimensional expressions  $(dF/da).(a/F)$  and  $(da/dh).(h/a)$ . The proposed paper is a contribution to the study of material elastoplastic properties evaluation by spherical indentation. Tabor’s relation or plastic similarity solution are used in various methodologies for mechanical property extractions through indentation experiment (Tabor 1951, Field and Swain 1995, Taljat et al. 1998, Ahn and Kwon 2001, Kucharski and Mroz 2001, 2004, 2007, Huber and E. Tyulyukovskiy 2003, Mulford et al. 2004, Weiler et al. 2005, Herbert et al. 2006, Jeon et al. 2006, Kim et al. 2006, Jiang et al. 2009, Zhang et al. 2009).  $\Psi$  and  $c^2$  parameters are used in Tabor’s relation and plastic similarity solution. Most of these methods were used with the assumption that the indentation regime is fully plastic. The results of the proposed work allow the validity of these methods in the case of weak strain hardened material to be determined.

## 2. Numerical procedure

Numerical simulations were principally performed with rigid parabolic indenter geometry, defined by the equation  $z = r^2/(2R)$ , where  $r$  and  $z$  are respectively the radial and the vertical coordinates and  $R$  is the radius of the osculatory circle. Several numerical simulations of spherical indentation were performed in order to examine the difference between the results

obtained for spherical indentation and parabolic indentation. These simulations were performed in axisymmetric mode and under frictionless contact conditions ( $\mu=0$ ) using the large strain elastic-plastic feature of the Abaqus finite element code. A typical mesh, comprising four-noded axisymmetric elements CAX4 (Abaqus, 1995), is shown in Fig. 1. In order to obtain precise values of contact radius throughout the indentation test, different numerical simulations were performed with parabolic indenters of  $R$  values chosen in the range of 0.316 to 316,000 mm ( $R=0.316, 1, 3.16, 10$  etc). Each finite element calculation was performed so that the final contact radius is equal to 1 mm. The dimensionless indentation curves  $a^*-F^*$  and  $h^*-a^*$  ( $a^*=a/R$  ;  $F^*=F/(E^*R^2)$ ,  $h^*=h/R$ ) were obtained by assembling the final parts of the different indentation curves obtained for each value of  $R$ . With this procedure, a minimum of 100 elements became directly in contact with the rigid indenter for each point of the indentation curves  $a^*-F^*$  and  $h^*-a^*$  used in this study. The mesh size was chosen so that, in all cases, the contact radius was 500 times smaller than the total length. According to the Hertz theory, good numerical results were obtained with this mesh size for the elastic indentation regime.

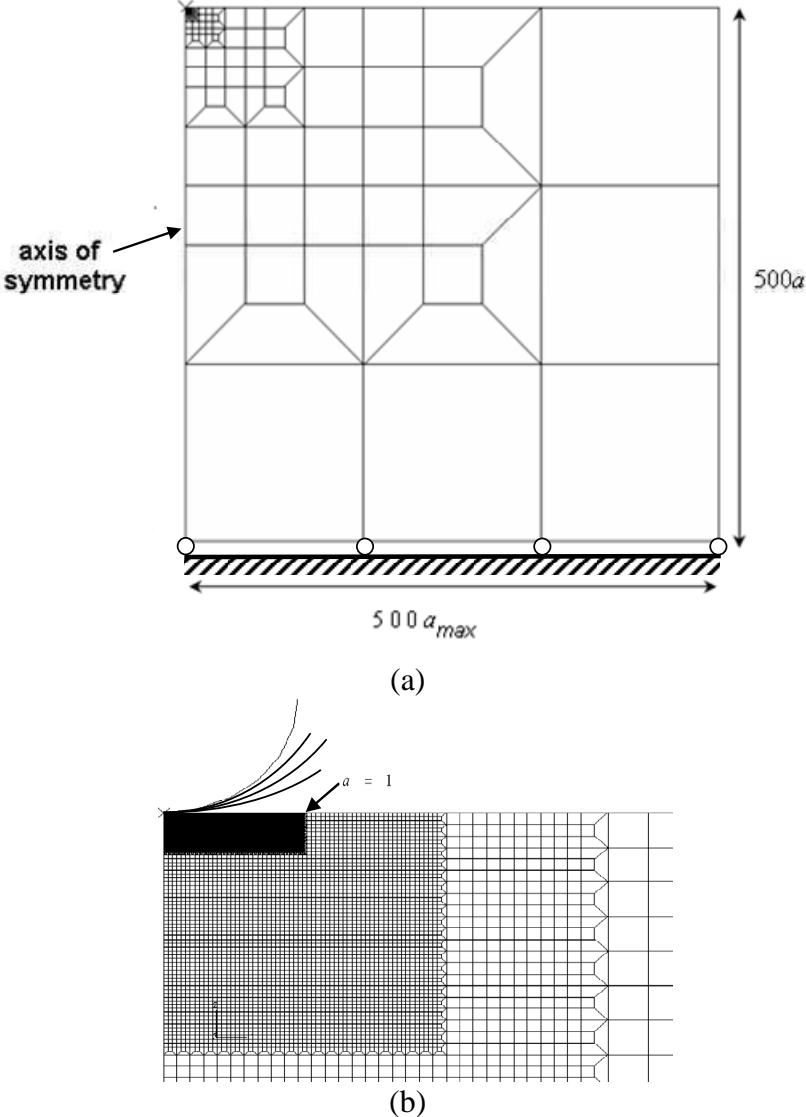


Fig. 1: Typical finite-element mesh, composed of four-noded axisymmetric elements and rigid parabolic indenters: (a) overall; (b) detail in the region of contact.

The constitutive model of the elastic-ideally plastic indented material was taken to follow the well known  $J_2$ -associated flow theory with rate-independent deformation.

Finite element simulations were performed for materials exhibiting values of  $\sigma_y = 0.105, 1.05, 10.5, 105, 1,050, 4,200$  and  $10,500$  MPa. Young modulus of 210 GPa and Poisson ratio of 0.3 are used for all simulations. These values were chosen in order to give  $\sigma_y/E$  ratio in the range of  $1/2,000,000-1/20$ , which includes most metals.

The actual contact radius  $a$  in our FE analysis depends of the horizontal coordinate of the last contact edge “node” between indenter and specimen. Because the actual contact radius is a discrete value and depends on the mesh size of contact surfaces, noisy  $(dF/da).(a/F)$  and  $(da/dh).(h/a)$  ratios were obtained starting from the FE results. A similar problem due to the discrete increments in contact size was found by Mesarovic and Fleck (1999).

In order to obtain non-noisy  $(dF/da).(a/F)$  and  $(da/dh).(h/a)$  ratios, fitted linear regression models with a least squares approach were used in different intervals of the  $\ln(a^*)-\ln(F^*)$  and  $\ln(h^*)-\ln(a^*)$  curves (Fig. 2). The interval used for the linear regression of each point  $X_i$  includes the closest to  $X_j$  points (denoted by square symbols in Fig. 2), such as:

$$X_i/\chi \leq X_j \leq \chi \cdot X_i \quad (1)$$

Where  $\chi$  is a constant which defines the length of the interval used to fit the linear regression model to the data.

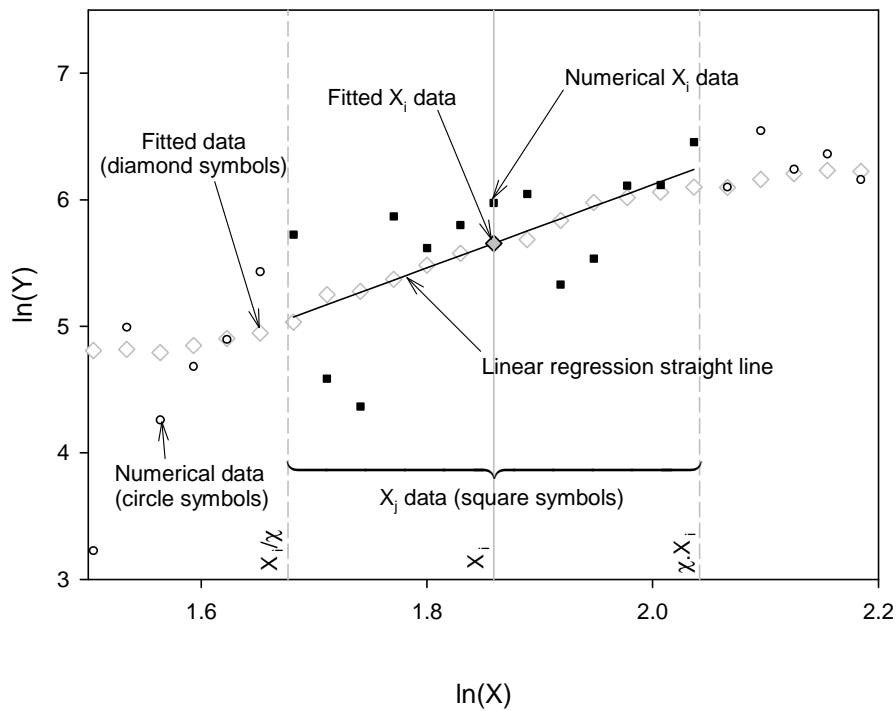


Fig. 2: Proposed method for smoothing the numerical data.

Examples of  $A-\psi$  and  $A-(dF/da).(a/F)$  relationships obtained by using the proposed method are shown in figure 3.

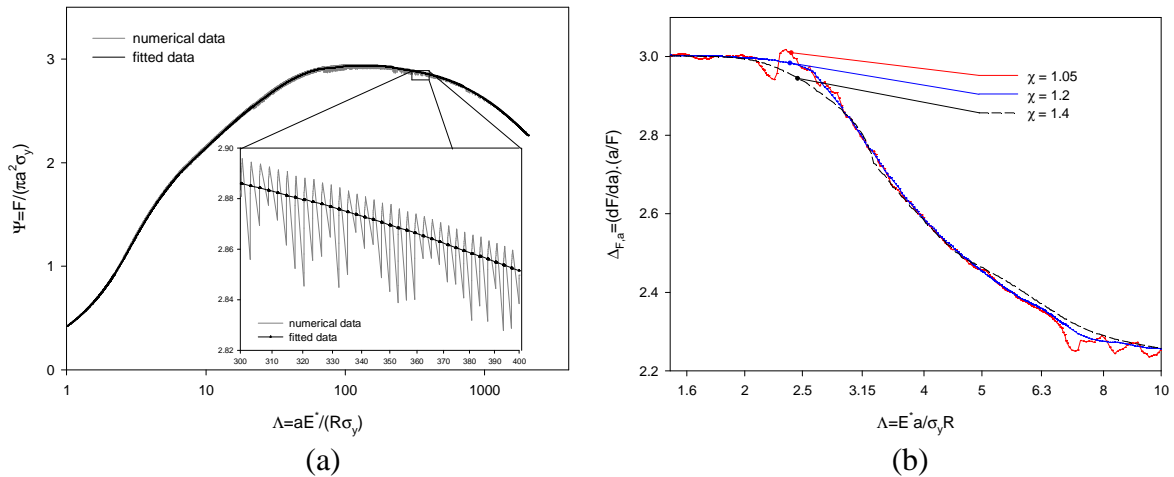


Figure 3: Numerical and fitted curve of  $\psi$  versus  $\Lambda$  obtained with  $\chi=1.2$  (a); fitted curves of  $\Lambda \cdot (dF/da) \cdot (a/F)$  obtained with various values of  $\chi$  (b); material of  $E/\sigma_y$  ratio equal to 2000.

For the results shown in Fig. 3b, various lengths of interval used for the linear regression were tested. The results show that the best fit for the data was obtained for a  $\chi$  parameter approximately equal to 1.2. For this reason, the value of  $\chi$  was fixed at 1.2 for all the fitted results.

Figure 4 shows a  $\Lambda \cdot (dF/da) \cdot (a/F)$  curve obtained by assembling the final parts of the different numerical results obtained for each value of indenter radius,  $R$ , and after fitting the linear regression model to the data. In this figure, the values of the coefficients of determination,  $r^2$ , are very close to 1 and thus indicate that the proposed model is a good fit.

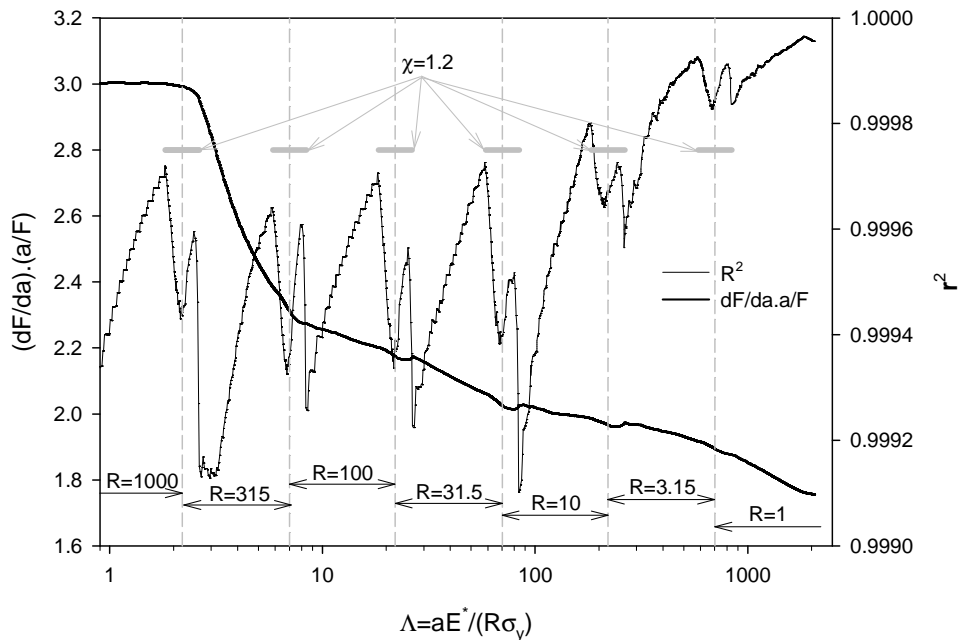


Figure 4:  $\Lambda \cdot (dF/da) \cdot (a/F)$  fitted curve and values of coefficients of determination obtained for a material of  $E/\sigma_y$  ratio equal to 2000 ( $\chi=1.2$ ).

Fig. 4 shows discontinuities in the assembled final  $\Lambda$ - $(dF/da).(a/F)$  curve at transitions between the numerical results obtained for each value of indenter radius,  $R$ . These discontinuities do not correspond to characteristic events during spherical indentation but are due to the low number of nodes in contact at the beginning of each finite element simulation. These discontinuities will not be taken into account in the study of  $(dF/da).(a/F)$  and  $(da/dh).(h/a)$  curves.

### 3. Parabolic indentation of elastic-ideally plastic materials of larger $E/\sigma_y$ ratio

Johnson (1985) argued that the degree of deformation in elastic-plastic indentation depends upon the ratio of the representative strain  $a/R$  beneath the indenter to the Yield strain  $\sigma_y/E^*$  of the half-space. Thus the degree of indentation is defined by the single non-dimensional group  $aE^*/R\sigma_y$ , which we shall name  $\Lambda$ . With this rationale in mind,  $(dF/da).(a/F)$  and  $(da/dh).(h/a)$  ratios are plotted versus  $aE^*/R\sigma_y$  in Fig. 5, for parabolic indentation and materials with large  $E/\sigma_y$  ratios.

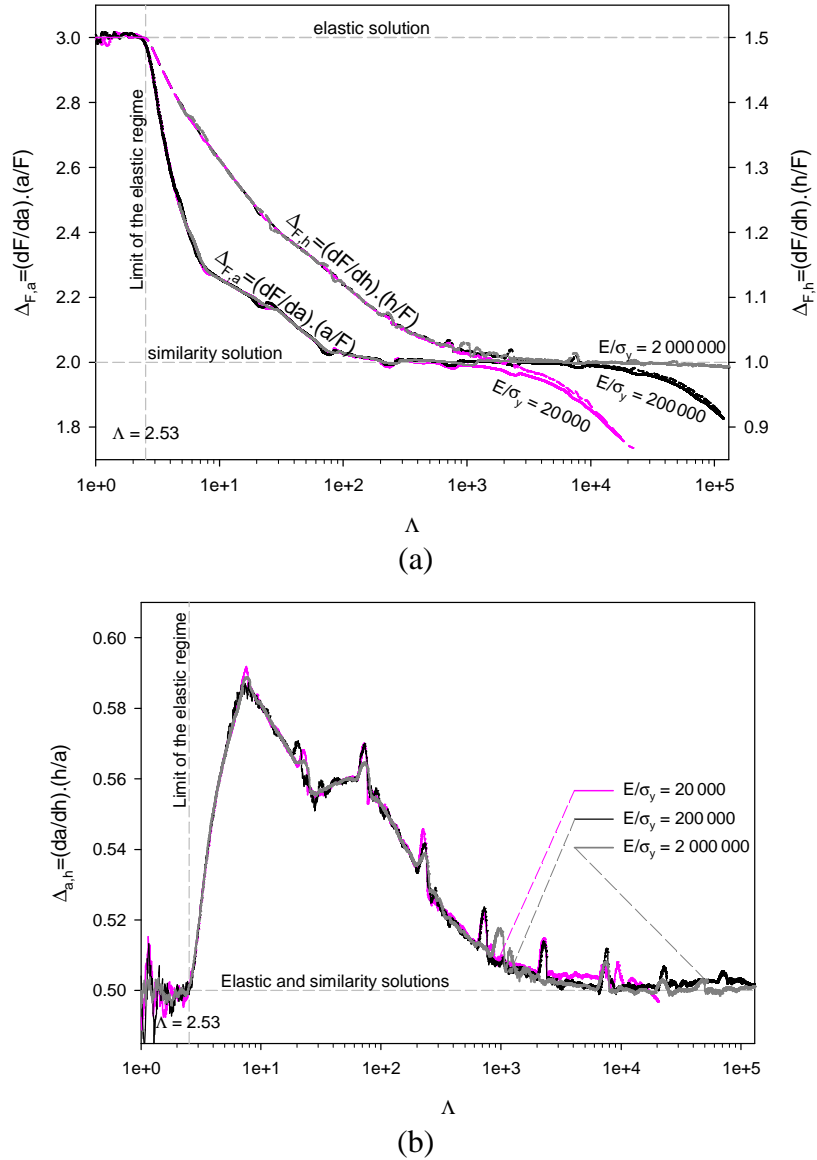


Fig. 5:  $(dF/da).(a/F)$ ,  $(dF/h).(h/F)$  and  $(da/dh).(h/a)$  ratios versus  $\Lambda = aE^*/R\sigma_y$  for materials of large  $E/\sigma_y$  ratio.

In these curves, different regimes can be distinguished. For small values of  $aE^*/R\sigma_y$ , the  $(da/dh).(h/a)$  and  $(dF/da).(a/F)$  ratios are constant and respectively 0.5 and 3, which correspond to the theoretical values of Hertz (1896). Starting from a critical value of  $aE^*/R\sigma_y$ , the  $(dF/da).(a/F)$  ratio decreases quickly then less quickly until it reaches the value of 2. When this value is reached,  $(dF/da).(a/F)$  stabilizes and then decreases again. The lower the  $E/\sigma_y$  ratio of the indented material, the earlier and steeper is the last decrease in  $(dF/da).(a/F)$ .

As for the  $(dF/da).(a/F)$  ratio, a big change in the  $(da/dh).(h/a)$  ratio occurs for the same values of  $aE^*/R\sigma_y$ . The  $(da/dh).(h/a)$  ratio increases quickly starting from the elastic regime and up to a value of  $\Lambda$  of about 8. Starting from  $\Lambda = 8$ , the  $(da/dh).(h/a)$  ratio decreases and when  $\Lambda$  is higher than approximately 10,000, the  $(da/dh).(h/a)$  tends towards the similarity solution, i.e. 0.5, without reaching this value for materials of  $E/\sigma_y$  ratio smaller than 200,000.

### 3.1 yielding of the material

In parabolic indentation, the elastic regime is valid up to a  $\Lambda$  parameter of 2.53. The  $(dF/da).(a/F)$  and  $(da/dh).(h/a)$  ratios show that the indentation regime is different from the elastic regime starting from a value of  $\Lambda$  which is very close to 2.53. This result is different to those presented by Park and Pharr (2004) and Mesarovic and Fleck (1999) in previous studies of the evolution of the constraint factor during spherical indentation. Indeed, these authors determined a ‘pseudo-Hertzian’ regime at the beginning of the yielding of the indented material. For Park and Pharr (2004), there is no deviation in behaviour from that expected based on purely elastic Hertzian contact over the range of approximately  $0 < \Lambda < 3.5$ . For Mesarovic and Fleck (1999), a ‘pseudo-Hertzian’ behaviour was found up to a value for  $\Lambda$  of 3.77. The  $\Lambda$ - $\psi$  relationship obtained with our numerical calculations for elastic-ideally plastic materials of different yield stress confirms that no ‘pseudo-Hertzian’ behaviour exists during parabolic and spherical indentation (Fig. 6). Indeed, this figure shows that the behaviour is rather different to that of Hertzian behaviour starting from the yielding of indented materials.

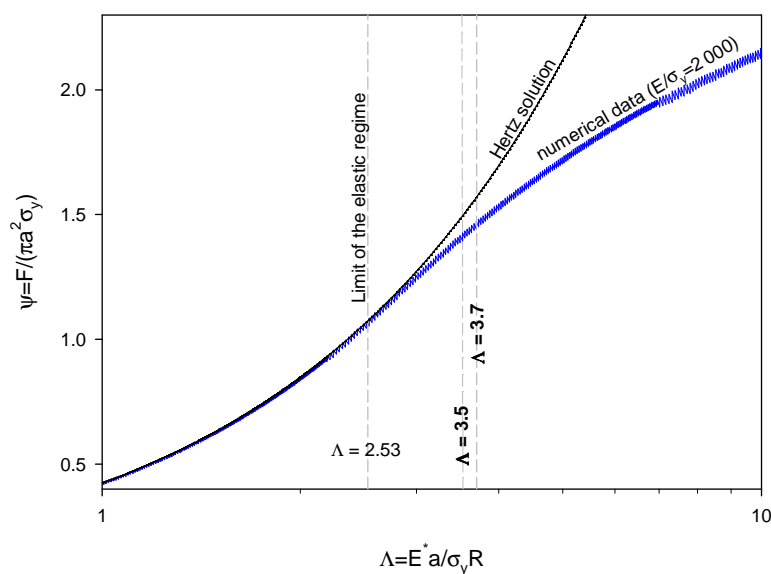


Fig. 6: Evolution of the constraint factor,  $\psi$  at the beginning of the yielding of the indented material

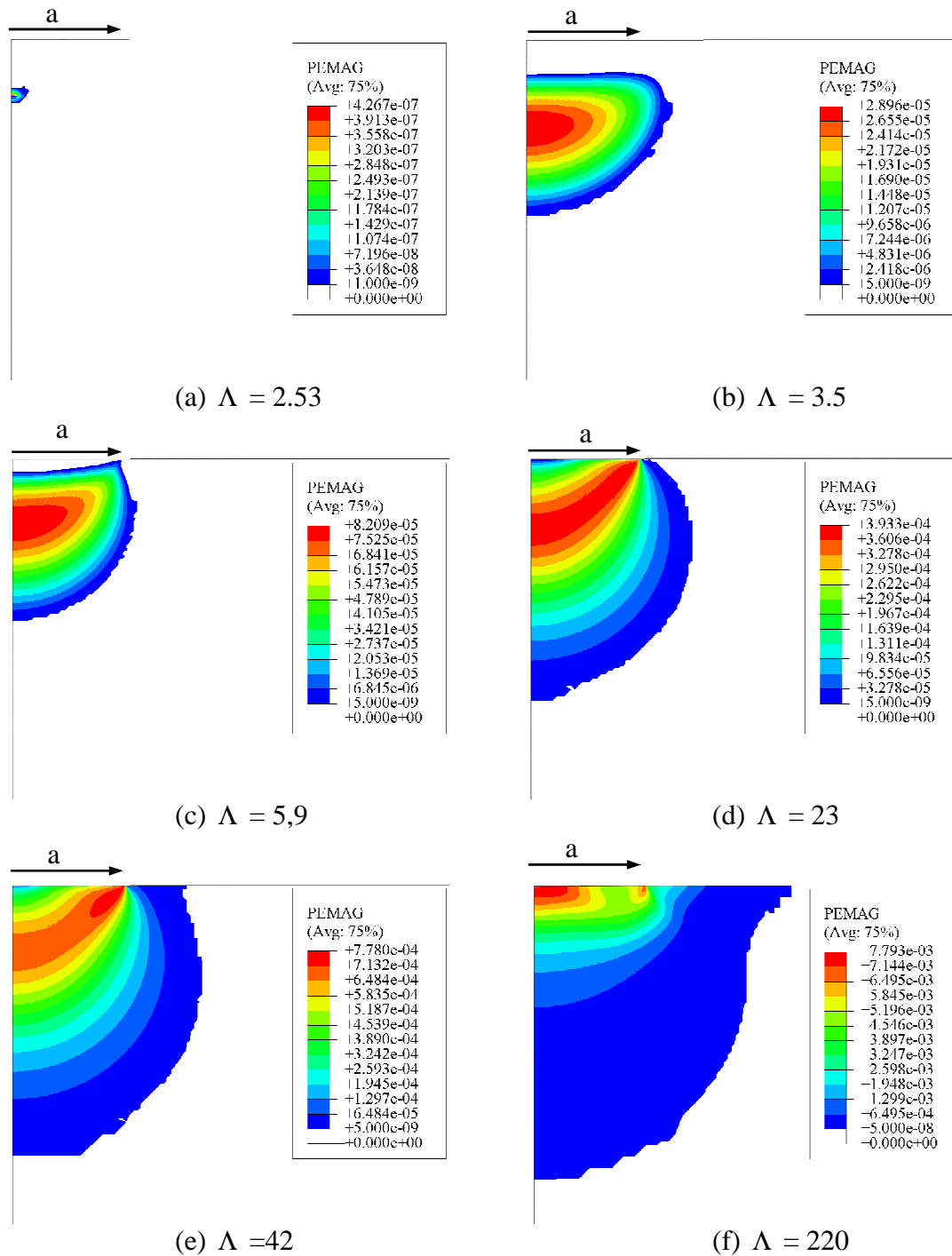


Fig. 7: Evolution of the plastic zone during the parabolic indentation of a material of  $E/\sigma_y=20000$  (PEMAG= plastic strain according to the Von Mises theory).  
a: yielding of the material; b: limit of the “pseudo-Hertzian” regime defined by Park and Pharr (2004) ; c: plastic zone first breaks through the surface ; d: yielding of the material at the whole surface contact ; e: maximum plastic strain located at the contact edge; f: maximum plastic strain located near the surface and the symmetry axis

It is also underlined that the reason of the existence of the “pseudo-Hertzian” behaviour given by Park and Pharr (2004) is not correct. For Park and Pharr (2004), the existence of the “pseudo-Hertzian” behaviour can be understood by considering the evolution of the plastic

zone. Their explanation is that as the plastic zone grows, it spreads upward and outward, but the plasticity is totally constrained by surrounding elastic material up to  $\Lambda = 3.5$  and at loads slightly greater than this, the plastic zone first breaks through the surface. Thus, the region of “pseudo-Hertzian contact occurs when  $2.52 < \Lambda < 3.5$ . As shown in Fig. 7, our results are not in accordance with the results of Park and Pharr because the plastic zone first breaks through the surface for a value of  $\Lambda$  greater than 3.5. For the different elastic-ideally plastic materials tested in this study, plasticity is totally constrained by surrounding elastic material when the  $\Lambda$  parameter is equal to 3.5 and 3.77 and the plastic zone first breaks through the surface when  $\Lambda$  is about 5.9 (Fig. 7.c). In consequence, the deviation in behaviour from that expected based on purely elastic Hertzian contact is not due to the break of the plastic zone through the surface.

### 3.2 Beginning of the plastic deformation

For  $aE^*/R\sigma_y > 2.53$ ,  $(dF/da).(a/F)$  decreases quickly and  $(da/dh).(h/a)$  increases quickly up to a value of  $aE^*/R\sigma_y$  of about 8 (Fig. 5), a value not far from that for which the plastic zone first breaks through the surface, i.e.  $aE^*/R\sigma_y = 5.9$  (Fig. 7). On the other hand, the study of the  $(dF/dh).(h/F)$  ratio shows that this parameter decreases gradually over the range of  $2.53 < \Lambda < 1000$  (Fig. 5.a). These results and the large changes in  $(dF/da).(a/F)$  and  $(da/dh).(h/a)$  observed at the first step of yielding indicate that the contact radius increases very quickly.

From  $\Lambda = 8$ , a decrease in  $(da/dh).(h/a)$  ratio is observed. From the same value of  $\Lambda$ , there is less decrease of  $(dF/da).(a/F)$ . These phenomena indicate that the speed of the piling-up formation decreases slightly. For Park and Pharr,  $aE^*/R\sigma_y = 10$  corresponds to the transition between an elastically-dominated regime and a plastically-dominated regime. For these authors,  $\Lambda = 10$  corresponds to the transition of two regimes, in which the indentation behaviour depends or not on the work hardening characteristics of the indented material. For our work, this explanation is not valid because the studied materials are elastic-ideally plastic. Fig. 8 shows rather that  $\Lambda = 12$  is a value which is very close to that given by Park and Pharr (2004) and corresponds to a modification of the location of the maximum plastic strain. When  $\Lambda$  is smaller than 12, the maximum plastic strain is located along the axis of the symmetry, in agreement with the Hertzian contact theory. Beyond this value, Fig. 8 shows that the indentation regime becomes very different from the elastic regime.

To resume, during the step corresponding to  $\Lambda$  values in the range of 2.53 and 12, the plastic zone grows beneath the surface, spreads upward and outward, breaks through the surface when  $\Lambda$  is about equal to 5.9, and is not constrained by surrounding elastic material at the end of the step (Fig. 7). The large changes in the plastic zone mean, consequently, large changes in the  $(dF/da).(a/F)$  and  $(da/dh).(h/a)$  ratios over the range of approximately  $2.53 < \Lambda < 8$  (Fig. 5). When  $\Lambda = 12$ , the location of the maximum plastic strain is not located along the axis of symmetry.

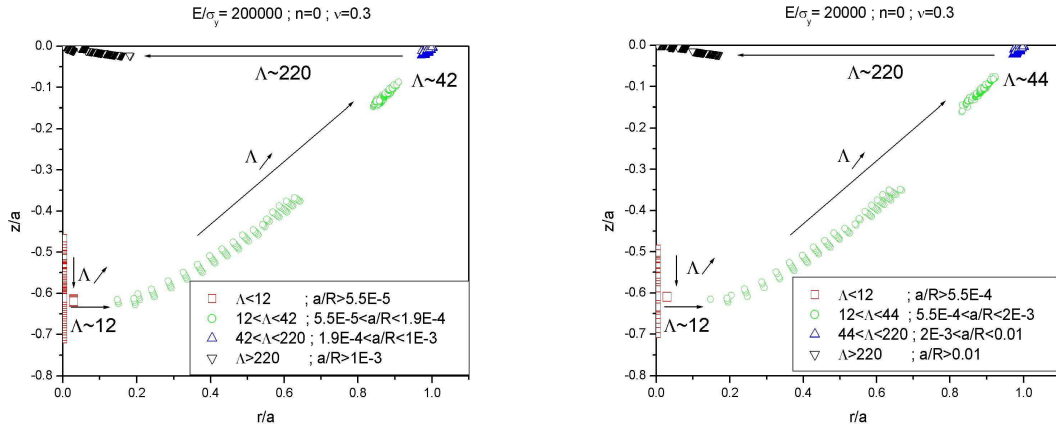


Fig. 8: Evolution of the localisation of the maximum plastic strain during parabolic indentation of materials of large  $E/\sigma_y$  ratio.

### 3.3 “elastic-plastic” and “fully plastic” regimes

For  $aE^*/R\sigma_y > 6-8$ , the  $(dF/da).(a/F)$  ratio decreases slowly up to a value of  $\Lambda$  of approximately 200 (Fig. 5.a). Fig. 8 shows that the maximum plastic strain location moves slowly upwards and outwards starting from  $\Lambda=12$  and is located at the contact edge when the value of  $\Lambda$  is equal to 220. When the maximum plastic strain moves toward the symmetry axis, i.e. for  $\Lambda$  values larger than 220, the  $(dF/da).(a/F)$  ratio and constraint factor,  $\psi$ , remain constant at values of 2 and 3 respectively, which correspond to the values of the rigid-ideally plastic similarity solution (Fig. 9.a). The values of  $\psi$  are close of the values determined by experimental investigations (O Neill, 1944; Tabor, 1951) or by finite element simulations (Mesarovic and Fleck, 1999; Park and Pharr, 2004). The value of  $\Lambda$  starting from  $\psi=3$  is in the range of the values determined by Park and Pharr (2004), i.e.:  $E^*a/(\sigma_y R) \approx 50$  to 200. On the other hand, this value is higher than those obtained by Johnson (1985),  $E^*a/(\sigma_y R) \approx 40$ ; Mesarovic and Fleck (1999),  $E^*a/(\sigma_y R) \approx 40-50$ ; Taljat and Pharr (2004),  $E^*a/(\sigma_y R) = 110$  and Pane and Blank (2006),  $E^*a/(\sigma_y R) = 80$ .

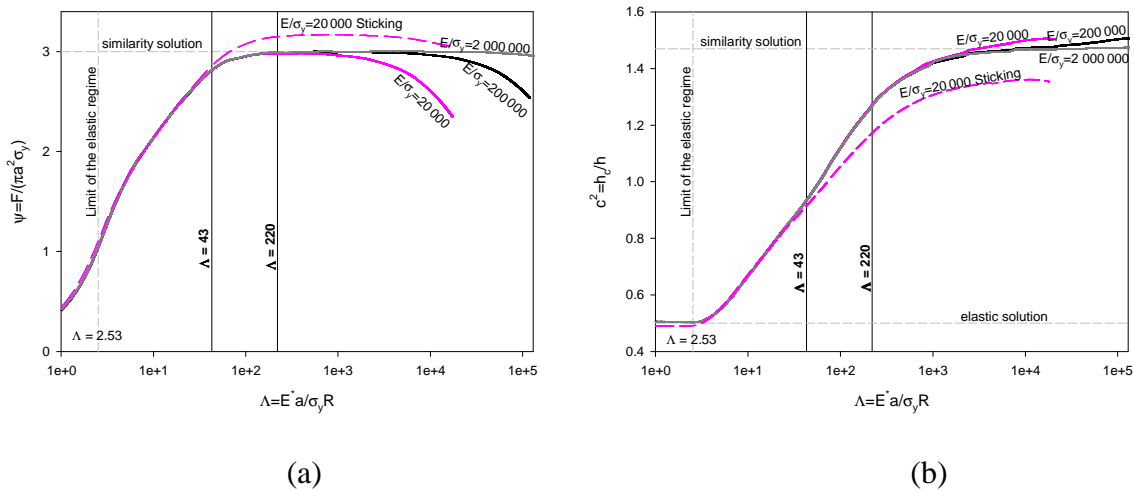


Fig. 9: Evolution of the constraint factor,  $\psi$ , and  $c^2$  parameter during parabolic indentation of materials of large  $E/\sigma_y$  ratio.

For  $aE^*/R\sigma_y > 12$ , the  $(da/dh).(h/a)$  ratio decreases slowly, but conversely to the  $(dF/da).(a/F)$  ratio is not constant starting from  $\Lambda = 220$  (Fig. 5.b).

When  $\Lambda$  is higher than 10,000,  $(da/dh).(h/a)$  tends towards the similarity solution, i.e. 0.5 (Fig. 5.b). Fig 9.b shows that the similarity solution, i.e.  $h_c/h=1.47$ , is attained for a material of  $E/\sigma_y$  equal to 2,000,000 when  $\Lambda$  is equal to 10,000. For materials of  $E/\sigma_y$  ratio smaller than 200,000, the  $c^2$  parameter increases quickly with  $\Lambda$  starting from the elastic regime and increases more slowly for values of  $\Lambda$  higher than about 200. This result shows that the models in which the  $c^2$  parameter is considered constant during a stage called “fully plastic regime” are not correct ((Matthews, 1980; Hill et al, 1989; Taljat et al., 1998; Alcalá et al., 2000).

Fig. 9 shows the effect of friction on the values of the similarity solutions. It is clear from Figs. 9.a and 9.b that the values of the similarity solutions in terms of  $\psi$  and  $h_c/h$  for the case of sticking indentation are respectively higher and smaller than those obtained for the case of frictionless indentation.

For high values of  $\Lambda$ , Fig. 5.a shows that the  $(dF/da).(a/F)$  ratio falls starting from the value of the similarity solution. For materials of an  $E/\sigma_y$  ratio equal to 200,000 and 20,000, the drop occurs respectively to values of  $\Lambda$  lower than 10,000 and 1,000. Fig. 9.a shows that the drop of the  $(dF/da).(a/F)$  ratio corresponds to the drop of the constraint factor,  $\psi$ . The same behaviour has been observed by Mesarovic and Fleck (1999) concerning the constraint factor,  $\psi$ . Fig. 9.b shows that the  $c^2$  parameter obtained for the material of  $E/\sigma_y$  ratio equal to 20,000 becomes higher than that obtained for the material of  $E/\sigma_y$  ratio equal to 200,000 for the same value of  $\Lambda$  corresponding to the drop of the  $(dF/da).(a/F)$  ratio and the constraint factor,  $\psi$ . The greater increase in the  $c^2$  parameter starting from a given value of the  $\Lambda$  parameter indicates that the formation of the piling-up is accentuated as the indentation continues. This result obtained for elastic-ideally plastic materials indented by a parabolic indenter is different from that obtained by Mesarovic and Fleck (1999) in the case of spherical indentation. Indeed, Mesarovic and Fleck (1999) found that the beginning of the finite deformation plasticity regime corresponds to the drop of the constraint factor,  $\psi$  and the  $c^2$  parameter. Moreover, the drop of the constraint factor,  $\psi$  does not correspond to that of the  $c^2$  parameter in the work of Mesarovic and Fleck (1999). No explanation was given by these authors. We will discuss about this point hereafter in the paragraph corresponding to the study of the spherical indentation.

#### 4. Parabolic indentation of elastic ideally plastic materials of smaller $E/\sigma_y$ ratio

Figs. 10a and 10b show that a drop in the  $(dF/da).(a/F)$  ratio and the constraint factor  $\psi$  occurs for materials of smaller  $E/\sigma_y$  starting from a value of  $\Lambda$ , which decreases with decreasing  $E/\sigma_y$ . Fig. 10c also confirms that the  $c^2$  parameter becomes higher than those of materials with higher  $E/\sigma_y$  ratios for a particular value of  $\Lambda$ . The same particular value is reached when the  $(dF/da).(a/F)$  and  $\psi$  curves separate from those obtained for a rigid plastic material. This phenomenon occurs during a second plastic regime which corresponds partly to the finite deformation plasticity defined by Mesarovic and Fleck (1999). It is further noted from Fig. 10b that the maximum value of the average pressure associated with the similarity solution is never attained for an elastic-ideally plastic material with a  $E/\sigma_y$  ratio lower than about 200,000. Fig. 10c confirms that no rigid-ideally plastic similarity regime of constant  $a^2/2hR$  is obtained during the parabolic indentation of an elastic-ideally plastic material with a  $E/\sigma_y$  ratio lower than about 200,000.

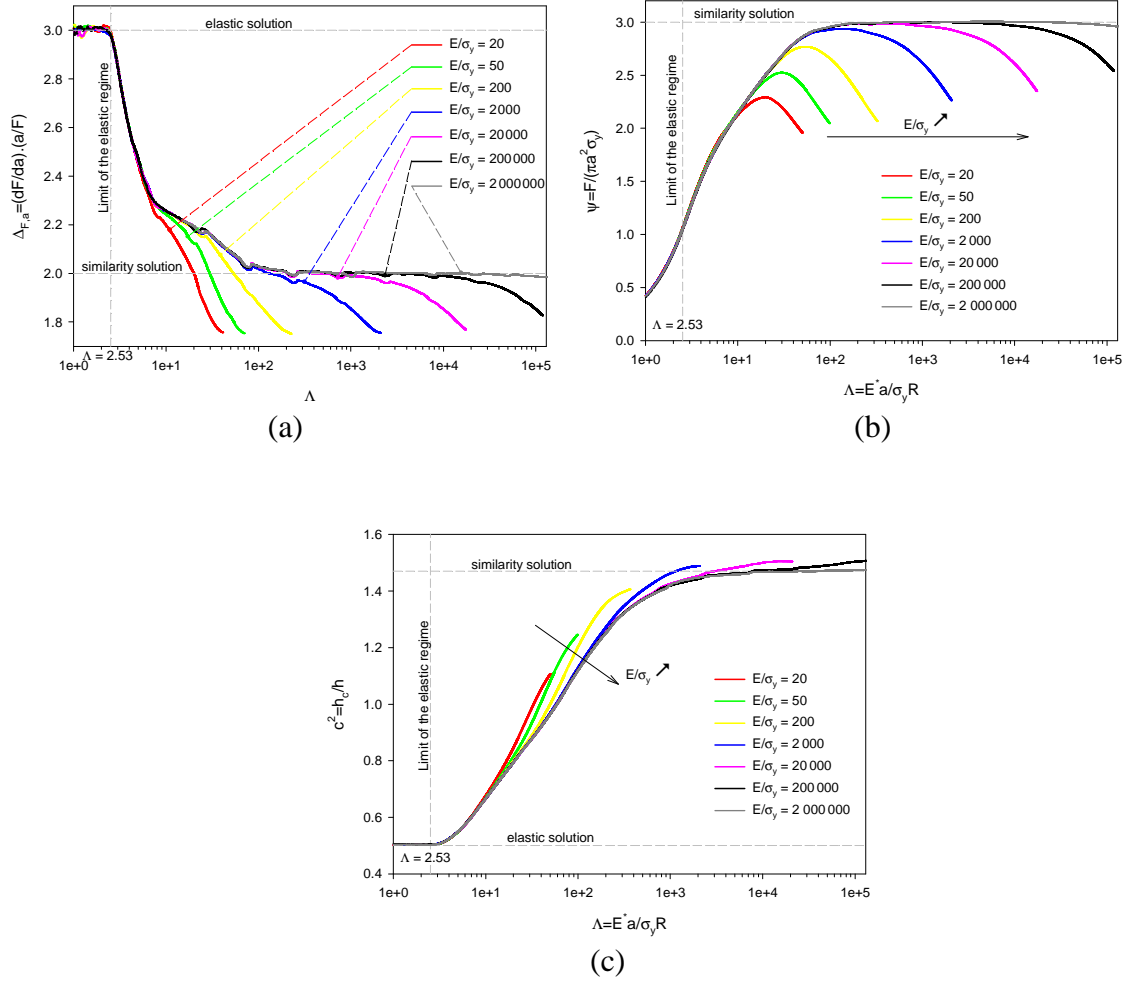


Fig. 10: Evolution of  $a/F.dF/da$ ,  $\psi$  and  $c^2=(h_c/h)$  as a function of  $\Lambda$ , during parabolic indentation of elastic-ideally plastic materials.

Fig. 11 shows the constraint factor,  $\psi$  and the  $c^2$  parameter changes according to the normalized contact size  $a/R$ . As was observed by Mesarovic and Fleck (1999), this figure shows that the curves of constraint factor,  $\psi$  versus  $a/R$  seem to coalesce to a single master curve when  $a/R$  increases. Close examination of the Fig. 11.a highlights a small difference between the curves obtained for materials of a small  $E/\sigma_y$  ratio (smaller than 200). The existence of a single master curve depending on the normalized contact size  $a/R$  indicates that the elastic contribution to the strain field beneath the indenter is negligible, and the parameter  $E^*a/(\sigma_y R)$  ceases to uniquely define the degree of indentation. For Mesarovic and Fleck (1999), the elastic contribution to the strain field beneath a spherical indenter is negligible for  $a/R > 0.16$ , independent of the magnitude of  $E/\sigma_y$ . Our results show that this is not the case for parabolic indentation. Indeed, the curves of the constraint factor,  $\psi$  versus  $a/R$  coalesce to a single master curve starting from a value of  $a/R$  depending on the  $E/\sigma_y$  ratio of the indented material. For the higher value of  $E/\sigma_y$  ratio, the constraint factor,  $\psi$  reaches the value of similarity solution in a first step and then falls starting from a very low value of normalized contact size  $a/R$  (lower than 0.01) following the master curve. The low value of the normalized contact size  $a/R$  starting from where the finite deformation regime occurs does not validate the definition of the finite deformation regime given by Mesarovic and Fleck (1999), i.e., “as the contact size increases, the tangential velocity of points in contact with the indenter deviates from the horizontal, so that the uniform vertical velocity boundary condition ceases

to be appropriate". For the lower value of  $E/\sigma_y$  ratio, the constraint factor,  $\psi$  doesn't reach the value of similarity solution and falls starting from a value of normalized contact size  $a/R$ , which increases with decreasing the value of the  $E/\sigma_y$  ratio of the indented material.

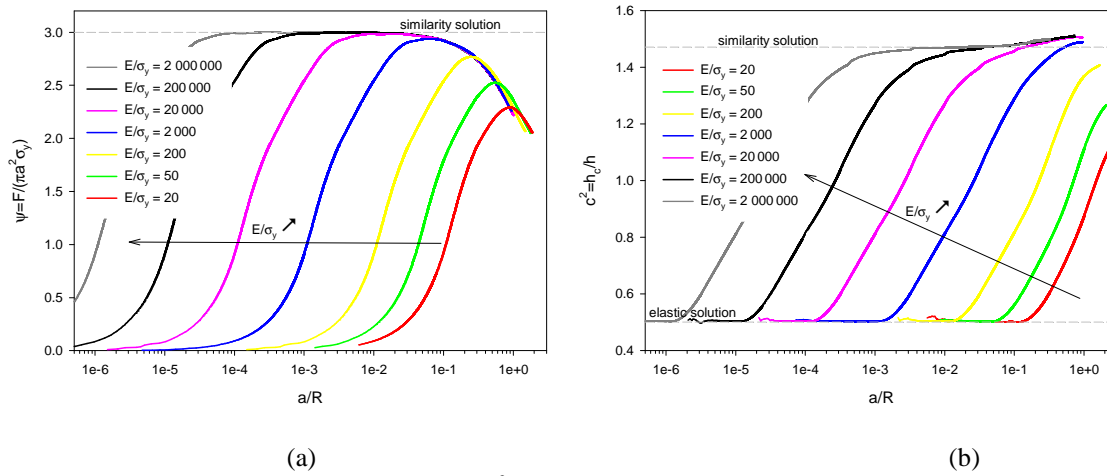


Fig. 11:  $\psi$  et  $c^2$  parameters as a function of  $a/R$ .

It was noticed, for materials of very high  $E/\sigma_y$  ratio ( $E/\sigma_y > 20,000$ ), that the constraint factor,  $\psi$  is close to the value of the similarity solution when the maximum plastic strain, located near the contact surface moves towards the symmetry axis (Fig. 8). For these materials, this phenomenon occurs starting from a value of  $\Lambda = 220$ . For materials of  $E/\sigma_y$  ratio lower than 20,000, the values of  $\Lambda$  starting from the plastic deformation reaches the contact edge and the symmetry axis decreases with decreasing  $E/\sigma_y$  (Fig. 12). In paragraph 4, the second plastic regime has been defined as being a regime where the constraint factor decreases and the  $c^2$  parameter increases more with an increase in  $\Lambda$ . Figs. 10 and 12 show that the maximum plastic strain is located near the contact surface and tends to move toward the symmetry axis when the second plastic regime occurs. For small values of  $E/\sigma_y$  ratio, the maximum plastic strain doesn't reach the contact edge before moving toward the symmetry axis because the second plastic regime occurs for low values of  $\Lambda$  (Figs. 12 c and d). The existence of the second plastic regime is due to the high values of the plastic strain located in periphery of the contact and to the greatest facility of material displacement on the surface. The combination of these two phenomena has as a consequence a decrease in the mean contact pressure and a higher increase in the piling-up (Figs. 10b and c). As the  $E/\sigma_y$  ratio of the indented material decreases, the different plastic regimes preceding the second plastic regime disappear and are replaced by this one.

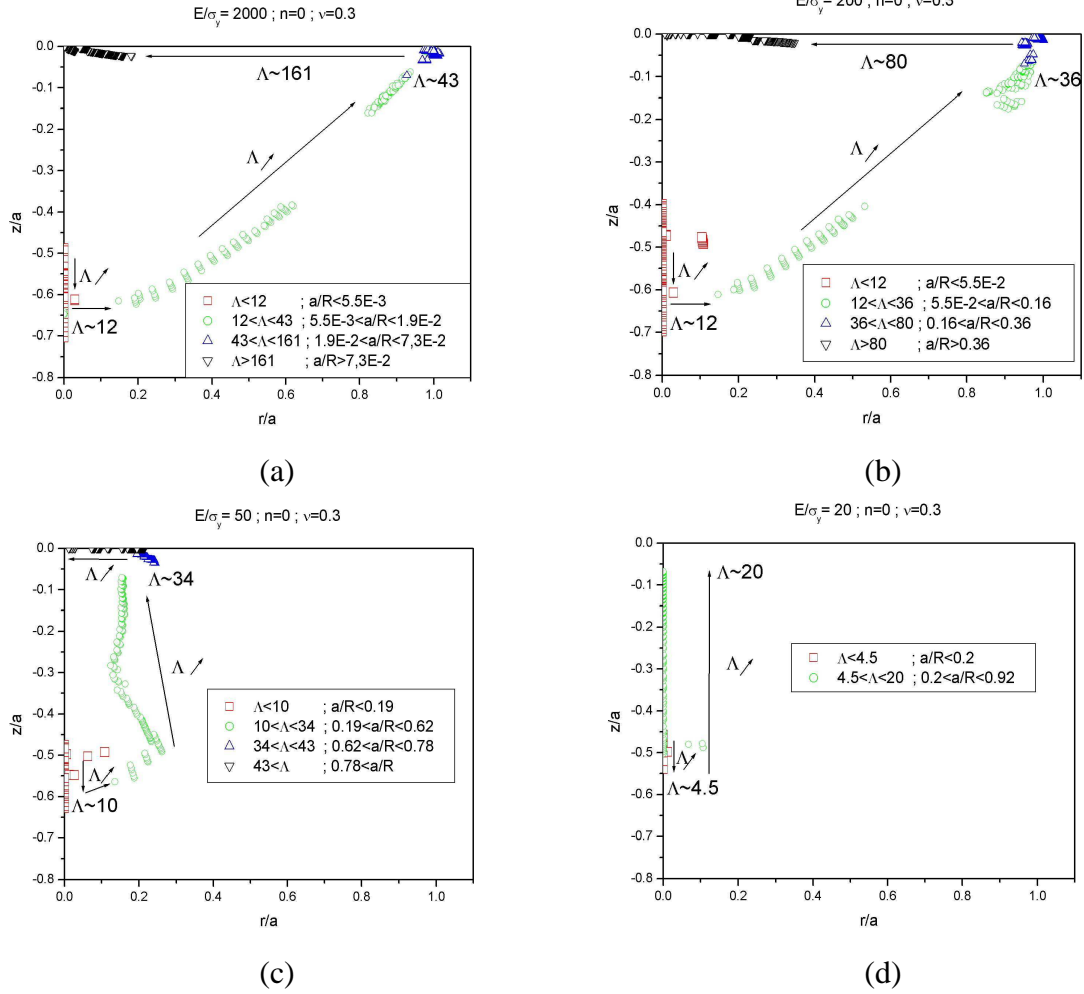


Fig. 12: Evolution of the localisation of the maximum plastic strain during parabolic indentation of materials of low and medium  $E/\sigma_y$  ratio.

Tabor (1951) proposed that the strain value on the edge of a spherical indentation of a given  $a/R$  is the “representative” strain of the indentation. Figs. 8 and 12 show that there is nothing particularly important or significant about the plastic strain on the indentation edge, as it is not always the maximum strain during plastic deformation. Nanoindentations carried out on the surface of annealed polycrystalline oxygen-free copper (OFC) of 99.99% purity, showed that the maximum strain hardening occurs in areas close to the centre of the indentations even for small  $a/R$  ratios (Chaudhri, 2000; Lim, 2002). Our results agree with these experimental results. Indeed, maximum plastic strain is found close to the centre of the indentations for small  $a/R$  ratios in the case of materials of large  $E/\sigma_y$  ratio (Figs. 8 and 12.a).

### 5. Spherical indentation of elastic ideally plastic materials.

Fig. 13 shows the changes of  $\psi$  and  $h_c/h$  with respect to  $\Lambda$ . Except for the last part of the curves, the comparison between this figure and Figs. 10b and 10c shows that results are similar to those obtained for the parabolic indentation. The same deformation regimes as those presented for parabolic indentation exist for spherical indentation.

For the final part of the curves shown in Fig. 13, the increase in  $\psi$  and the decrease in  $h_c/h$  are due to the loss of contact between the indented material and the indenter when the value of the contact radius is close to that of the indenter radius.

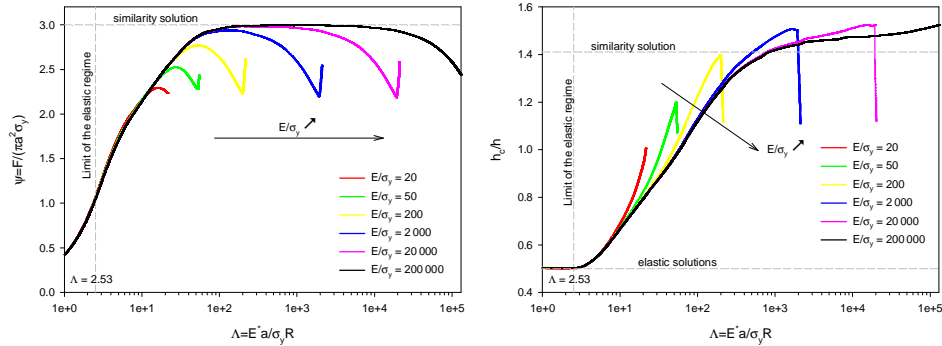


Fig. 13: Constraint factor,  $\psi$  and Contact depth-penetration depth ratio versus  $\Lambda$  for spherical indentation.

A more precise comparison between spherical and parabolic indentations is presented in Fig. 14 in the case of elastic-ideally plastic materials of  $E/\sigma_y$  ratios equal to 200 and 2,000.

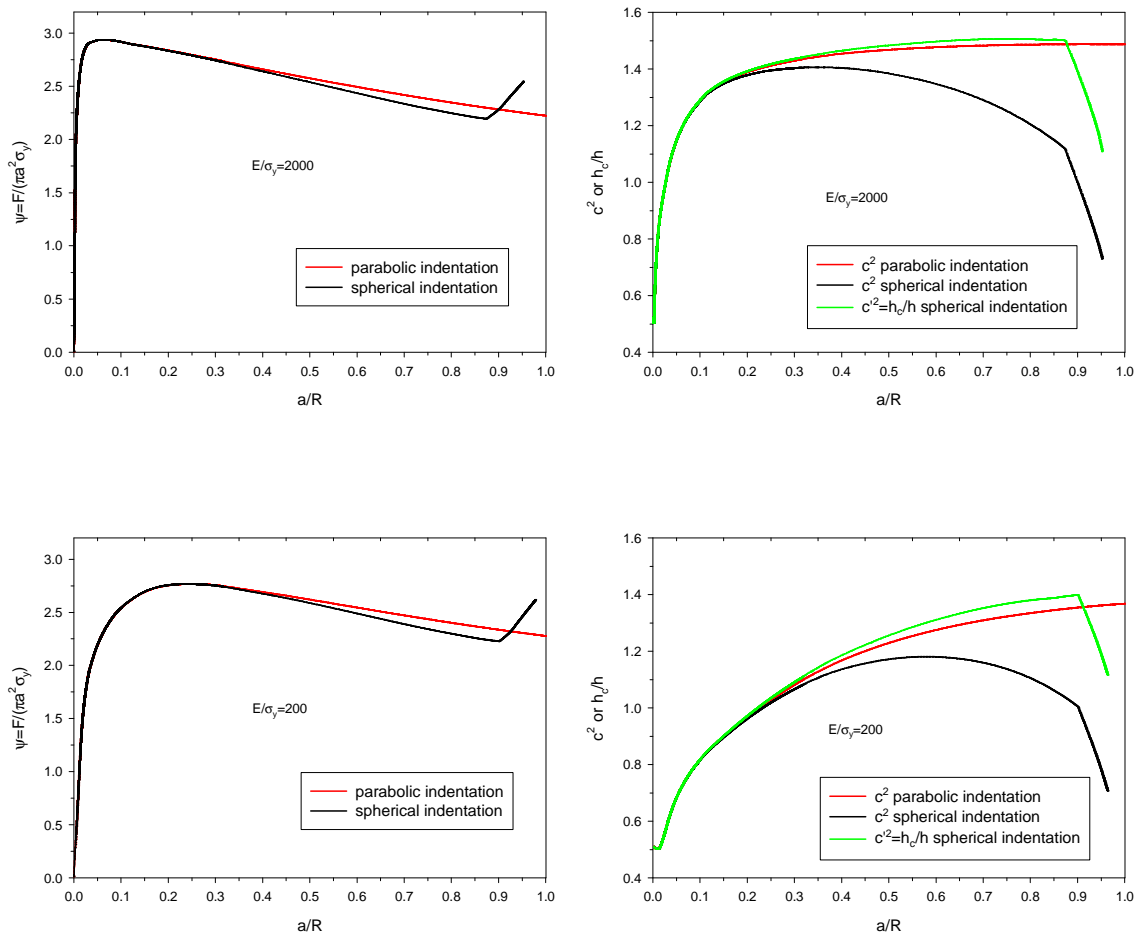


Fig. 14: Comparison between spherical and parabolic indentations of elastic ideally plastic materials of  $E/\sigma_y$  ratios equal to 200 and 2000.

Fig. 14 shows that the difference between the values of  $c^2$  obtained for spherical indentation and parabolic indentation is significant starting from values of non-dimensional contact radii higher than approximately 0.2. Note that the  $c^2$  parameter is equal to  $a^2/(2hR)$  in our study. In the case of parabolic indentation, this parameter corresponds to the ratio between the contact depth,  $h_c$ , and the penetration depth,  $h$ . The  $c^2$  parameter was also often used in previous studies to determine the degree of the piling-up or sinking-in in the case of spherical indentation (Mathews, 1980; Hill et al., 1989; Biwa and Störackers, 1995; Taljat et al., 1998; Mesarovic and Fleck, 1999; Alcala et al. 2000; Kucharski and Mröz, 2001). However, this parameter, which is valid for all values of contact radius in the case of parabolic indentation, is incorrect for high values of contact radius in the case of spherical indentation.

We showed in a previous study that the use of this parameter in the case of spherical indentation had, as a consequence, a large underestimation of the contact radius for high values of penetration depth (Hernot et al., 2006). In order to obtain a correct value of the  $h_c/h$  ratio, it is necessary to use the following parameter, called  $c'^2$ , when the profile of the spherical indenter cannot be approximated by a paraboloid of revolution:

$$c'^2 = \frac{h_c}{h} = \frac{R - \sqrt{R^2 - a^2}}{h} \quad (2)$$

Fig. 14 confirms that the  $c^2$  parameter has consequently a significant underestimation of the piling-up for large contact radius in spherical indentation. Moreover, the examination of the evolution of the  $c'^2$  parameter and of the  $c^2$  parameter obtained for the parabolic indentation shows that the difference between the results obtained for parabolic indentation and spherical indentation becomes significant starting from a value of  $a/R$  of approximately 0.3. This result is similar to that obtained for the  $\psi$  parameter.

In paragraph 3, we indicated that Mesarovic and Fleck (1999) did not explain in their work why the decreases in the constraint factor,  $\psi$ , and in the  $c^2$  parameter do not begin from the same value of  $\Lambda$ . The above results explain this. The decrease in the constraint factor is due to the decrease in contact pressure during the indentation test. The decrease in  $\psi$  occurs starting from a value of  $\Lambda$ , which depends on the indented material. The decrease in  $c^2$  is only due to the incorrect formulation of this parameter which is used to characterize the changes in piling-up or sinking-in.

On the basis of their numerical results, Mesarovic and Fleck (1999) defined the “finite-deformation plasticity regime” as being a regime in which the constraint factor,  $\psi$  and the  $c^2$  parameter decrease. However, the  $c^2$  parameter is not valid when it decreases and thus the definition of this regime is erroneous. The parabolic and spherical results presented given in Figs. 10b, 10c, and 13 show that this regime must be replaced by a regime, called in this article second plastic regime, in which the average pressure decreases ( $\psi$  decreases) and the formation of the piling-up is accentuated (greater increase in the  $h_c/h$  ratio).

## 6. Conclusion

The different deformation regimes during parabolic and spherical indentation of elastic-ideally plastic material are defined starting from the numerical study of the evolution of  $(dF/da).(a/F)$ ,  $\psi$ ,  $(da/dh).(h/a)$  and  $h_c/h$  versus the single non-dimensional group,  $\Lambda = E^* a / \sigma_y R$  and the non-dimensional contact radius,  $a/R$ . The study of the changes in the  $(dF/da).(a/F)$  and the  $(da/dh).(h/a)$  ratios indicates that, when the yield stress of an elastic-ideally plastic material is exceeded, several deformation regimes can exist according to the value of the  $E/\sigma_y$  ratio of the indented material.

For materials having a very large  $E/\sigma_y$  ratio, two elastic-plastic regimes and two plastic regimes were found. A first elastic-plastic regime is observed up to a  $\Lambda$  value of approximately 6-12. During this stage, the maximum plastic strain is located on the axis of symmetry and the  $(dF/da).(a/F)$  and  $(da/dh).(h/a)$  ratios change a lot because of the large changes in the plastic zone. The second elastic-plastic regime corresponds to a weak decrease in  $(dF/da).(a/F)$  up to a  $\Lambda$  value of approximately 220. During this step, no large modification of the plastic zone is found but the maximum plastic strain location moves slowly upwards and outwards and then remains located at the contact edge. For the first plastic regime, the  $(dF/da).(a/F)$  ratio and constraint factor,  $\psi$ , remain constant at values of 2 and 3 respectively, which correspond to the values of the rigid-ideally plastic similarity solution. The study of the  $(da/dh).(h/a)$  and  $h_c/h$  ratios shows that no rigid-ideally plastic similarity regime of constant  $h_c/h$  is obtained for materials of  $E/\sigma_y$  ratio smaller than 200,000. For these materials, the  $h_c/h$  ratio tends towards the similarity solution, i.e. 1.47, without reaching this value. For materials of  $E/\sigma_y$  ratio higher than 200,000,  $h_c/h$  and  $\psi$  are constant when  $\Lambda=10,000$ .

For the second and last plastic regime, the mean contact pressure decreases and the piling-up increases even more. This decrease in the mean contact pressure and this higher increase in the piling-up are more marked in the case of the spherical indentation. For materials of very high  $E/\sigma_y$  ratio, the second plastic regime appears when  $a/R$  is lower than 0.01. The low value of the normalized contact size  $a/R$ , from which the second plastic regime starts, shows that this regime is not related to a change of the direction of the tangential velocity of the points in contact with the indenter, as it was stated by Mesarovic and Fleck (1999).

The existence of the second plastic regime is due to the high values of the plastic strain located in the periphery of the contact and to the greatest facility of material displacement on the surface. The combination of these two phenomena leads to a decrease in the mean contact pressure and a steeper increase in the piling-up. The results of the finite element calculus show that the first plastic regime exists during spherical and parabolic indentation only for elastic-ideally plastic materials of an  $E/\sigma_y$  ratio higher than approximately 2000. The comparison of the results obtained for parabolic and spherical indentation shows that the  $c^2$  parameter generally used in order to characterize the evolution of the piling-up or the sinking-in in the case of spherical indentation is not correct beyond a value of a non-dimensional contact radius,  $a/R$  equal to about 0.2. When  $a/R$  is higher than 0.2, it is necessary to use the  $c'^2$  parameter ( $c'^2=h_c/h$ ), equal to the true contact depth-penetration depth ratio, in order to correctly determine the contact radius. To conclude, the complexity of the changes in the  $(dF/da).(a/F)$ ,  $\psi$ ,  $(da/dh).(h/a)$  and  $h_c/h$  parameters shows that it is not easy to determine simple relationships between the penetration depth,  $h$ , the contact radius,  $a$ , and the applied load,  $F$ , when an elastic-ideally plastic material is deformed by a sphere or a parabola. Particularly, this study shows that the  $a-h$  power laws, proposed in the literature, are incorrect with respect to their representation of the contact radius – depth penetration relationship. This work shows that both Tabor's relation and plastic similarity solution can not be used for mechanical property extractions, through spherical indentation, in the case of material with very weak strain hardening and  $E/\sigma_y$  ratio higher than approximately 2000. The results show that the non-dimensional expressions  $(dF/da).(a/F)$  and  $(da/dh).(h/a)$  are applicable for the study of the indentation regimes during spherical indentation of elastic-ideally plastic materials. This work is a first step before the study of the indentation regimes of work hardened materials during spherical indentation, using the non-dimensional expressions  $(dF/da).(a/F)$  and  $(da/dh).(h/a)$ . The advantage of these expressions is that they do not need the definition of a "representative" strain, which is needed in the case of  $\psi$ ."

## References

- Abaqus V6.5 user's manual, 1995.
- Ahn, J.H., Kwon, D., 2001. Derivation of plastic stress–strain relationship from ball indentations: Examination of strain definition and pileup effect. *J. Mater. Res.* 16 (11), 3170-3178.
- Alcala, J., Barone, A.C., Anglada, M., 2000. The influence of plastic hardening on surface deformation modes around Vickers and spherical indents. *Acta Mater.* 48, 3451-3464.
- Biwa, S., Stôrackers, B., 1995. An analysis of fully plastic Brinell indentation. *J. Mech. Phys. Solids* 43 (8), 1303-1333.
- Bower, A.F., Fleck, N.A., Needleman, A., Ogbonna, N., 1993. Indentation of a power law creeping solid. *Proc. R. Soc. Lond. A.* 441, 97–124.
- Chaudhri, M.M., 2000. Strain Hardening around Spherical Indentations. *Phys. Stat. Sol. (a)* 182, 641-652.
- Field, J. S., Swain, M. V, 1995. Determining the mechanical properties of small volumes of material from submicrometer spherical indentations. *J. Mater. Res.* 10, 101-112.
- Herbert, E.G., Oliver, W.C., Pharr, G.M., 2006. On the measurement of yield strength by spherical indentation, *Phil. Mag.* 86, 5521-5539.
- Hernot, X., Bartier, O., Bekouche, Y., Mauvoisin, G., El Abdi, R., 2006. Influence of Penetration Depth and Mechanical Properties on Contact radius Determination for Spherical Indentation. *Int. J. Solids Struct.* 43, 4136-4153.
- Hertz, H., 1881. Ueber die Berührung fester elastischer Körper. *Journal für die reine und angewandte Mathematik* 92, 156-171.
- Hill, R., Stôrakers, B., Zdunek, A.B., 1989. A theoretical study of the Brinell hardness test. *Proc. R. Soc. Lond. A* 423, 301-330.
- Huber, N., Tyulyukovskiy, E., 2003. A new loading history for identification of viscoplastic properties by spherical indentation *J. Mater. Res.* 19, 101-113.
- Ishlinsky, A.J., 1944. Axisymmetric plastic flow in the Brinell test. *Prikladnaya Matematika i Mekhanika* 8, 201–224.
- Jeon, E.C., Kima, J. Y., Baik, M.K., Kim, S. H., Park, J.S., Kwon, D, 2006. Optimum definition of true strain beneath a spherical indenter for deriving indentation flow curves. *Mater. Sci. Eng. A* 419, 196–201.
- Jiang, P., Zhang, T., Feng, Y., Yang, R., Liang, N., 2009. Determination of plastic properties by instrumented spherical indentation: Expanding cavity model and similarity solution approach. *J. Mater. Res.* 24, 1045-1053.
- Johnson, K.L., 1985. *Contacts Mechanics*. Cambridge University Press, Cambridge, UK.
- Kim, J.Y., Lee, K.W., Lee, J.S., Kwon, D., 2006. Determination of tensile properties by instrumented indentation technique: Representative stress and strain approach. *Surf. Coat. Tech.* 201, 4278–4283
- Kucharski, S., Mröz, Z., 2001. Identification of plastic hardening parameters of metals from spherical indentation tests. *Mater. Sci. Eng. A* A318, 65-76.
- Kucharski, S., Mröz, Z., 2004. Identification of material parameters by means of compliance moduli in spherical indentation test. *Mater. Sci. Eng. A* 379, 448–456.
- Kucharski, S., Mröz, Z., 2007. Identification of yield stress and plastic hardening parameters from a spherical indentation test. *Int. J. Mech. Sci.* 49, 1238–1250
- Lim, Y.Y., Chaudhri, M.M., 2002. Nanohardness Mapping of the Curved Surface of Spherical Macroindentations in Fully Annealed Polycrystalline Oxygen-Free Copper. *Phys. stat. sol. (a)* 194, 19-29.
- Matthews, J.R., 1980. Indentation hardness and hot pressing. *Acta Met.* 28, 311-318.
- Mesarovic, D.J., Fleck, N.A., 1999. Spherical indentation of elastic-plastic solids. *Proc. R. Soc. Lond. A* 455, 2707-2728.

- Mulford, R., Asaro, R., J., Sebring, R., J., 2004. Spherical indentation of ductile power law materials. *J. Mater. Res.* 19, 2641-2649.
- O'Neill, H., 1944. The significance of tensile and other mechanical test properties of metals. *Proc. Inst. Mech. Engrs.* 151, 116-130.
- Park, Y.J., Pharr, G.M., 2004. Nanoindentation with spherical indenters: finite element studies of deformation in the elastic-plastic transition regime. *Thin Solid Films* 447-448 (30), 246-250.
- Pane, I., Blank, E., 2006. Role of plasticity on indentation behaviour: Relations between surface and subsurface responses. *Int. J. Solids Struct.* 43, 2014-2036.
- Sundararajan, G., Tirupataiah, Y., 1994. The hardness-flow stress correlation in metallic materials. *Bull. Mater. Sci.* 17 (6), 747-770.
- Tabor, D., 1951. *The hardness of Metals*. Clarendon Press, Oxford, UK.
- Taljat, B., Pharr, G.M., 2004. Development of pile-up during spherical indentation of elastic-plastic solids. *Int. J. Solids Struct.* 41, 3891-3904.
- Taljat, B., Zacharias, T., Kosel, T., 1998. New analytical procedure to determine stress-strain curve from spherical indentation data. *Int. J. Solids Struct.* 35 (33), 4411-4426.
- Weiler, J., P., Wood, J. T., Klassen, R. J., Berkmortel, R., Wang, G., 2005. The effect of grain size on the flow stress determined from spherical microindentation of die-cast magnesium AM60B alloy. *J. Mater. Sci.* 40, 5999-6005.
- Zhang T., Jiang P., Feng Y., Yang R., Numerical verification for instrumented spherical indentation techniques in determining the plastic properties of materials. *J. Mater. Res.* 24, 3653-3663.